Supplementary Information

A thin, intrinsically stretchable MXene-MWCNTs/Polymer current collector for deformable aqueous Li-ion battery

Zi-Fang Chen,[abc] Xingguang Chen,[abc] Chengwei Chen,[abc] Xiaoxu Lai,[abc] Jian Qin,[abc] Chi Chen,[*abc] and Dan Sun[*abc]

[a] CAS Key Laboratory of Design and Assembly of Functional Nanostructures, and Fujian Provincial Key Laboratory of Nanomaterials, Fujian Institute of Research on the Structure of Matter, Chinese Academy of Sciences, Fuzhou, Fujian 350002, China

[b] Xiamen Institute of Rare Earth Materials, Haixi Institutes, Chinese Academy of Sciences, Xiamen, Fujian 361021, China

[c] Xiamen Key Laboratory of Rare Earth Photoelectric Functional Materials, Xiamen, Fujian 361021, China

[*] Corresponding authors.

E-mail addresses: xmsundan@fjirsm.ac.cn, xmchenchi@fjirsm.ac.cn.

Supplemental Experimental Section

Preparation and optimization of SEBS films

SEBS films with different thickness of about 89 μm, 110 μm, 144 μm, 180 μm, and 243 μm were prepared by dissolving different mass of SEBS particles in a mixture of THF and toluene. The volume ratio of THF and toluene is 5:3. To explore the resilience of SEBS after repeated stretching, SEBS samples with dumbbell shape were repeated 200% stretching for 10 times. As shown in Fig. S1, the SEBS film of about 89 μm presented a partial irreversible length and poor resilience. Moreover, stress-strain tests (Fig. S2) of SEBS films with 110 μm, 144 μm, and 180 μm showed that SEBS with 110 μm possesses both weak Young's modulus (15.5 Mpa) and tensile strength (9.87 Mpa), while the SEBS film with 144 μm and 180 μm exhibit similar mechanical properties. Since thinner batteries can be better assembled into wearable devices, we choose the SEBS of about 144 μm as a stretchable substrate.

Preparation and optimization of $Ti_3C_2T_x$-MWCNTs layers

$Ti_3C_2T_x$-MWCNTs ink composed of different volume ratios of $Ti_3C_2T_x$ (10 mg mL^{-1}) and MWCNTs ink (2 mg mL^{-1}) were prepared and deposited on SEBS film varying from 8:1, 4:1, 2:1 to 1:1. To investigate the effect of proportions on electrical conductivity, the superficial sheet resistance (Rs) of the each $Ti_3C_2T_x$-MWCNTs layers were tested under 20% strain and presented in Fig. S3. The normalized sheet resistance curves show that a certain amount of WMCNTs can improve the toughness of the conductive layer, but too much MWCNTs will cause the resistance to increase during stretching. Moreover, the surfaces of the released $Ti_3C_2T_x$-MWCNTs layers were also compared in Fig. S4. SEM images show that too many MWCNTs will cause surface agglomeration and protrusion, while too few carbon nanotubes have poor surface toughness and are prone to cracking. Combined with the results in Fig. S3, we believe that 4:1 is the best ratio.

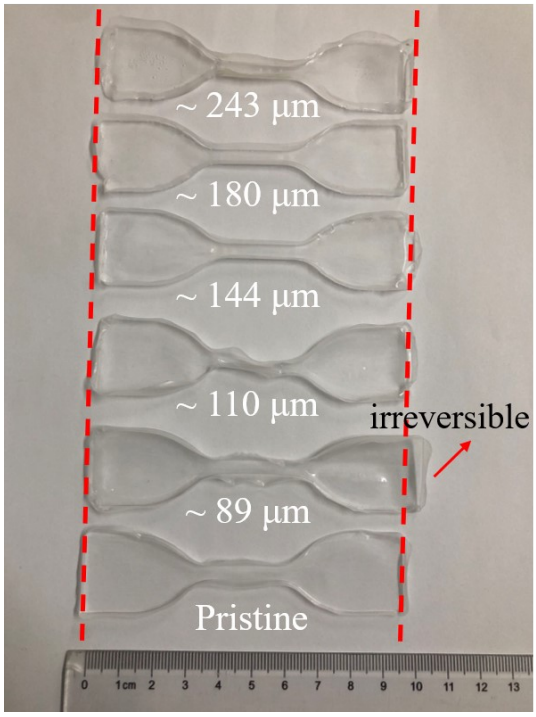

Fig. S1 SEBS samples after repeated 200% stretching (10 cycles).

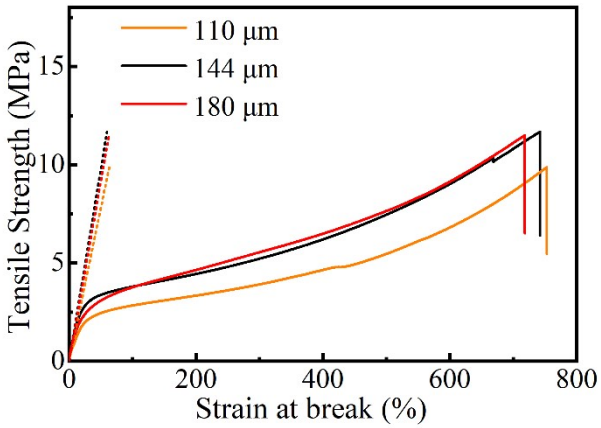

Fig. S2 Stress-strain tests of the SEBS films with different thicknesses.

Table S1. Mechanical properties of SEBS films with different thicknesses

Sample	Young's Modulus (MPa)	Tensile Strength (MPa)	Strain at break (%)
110 µm	15.5	9.87	753.21
144 µm	19.19	11.68	742.28
180 µm	18.20	11.51	718.61

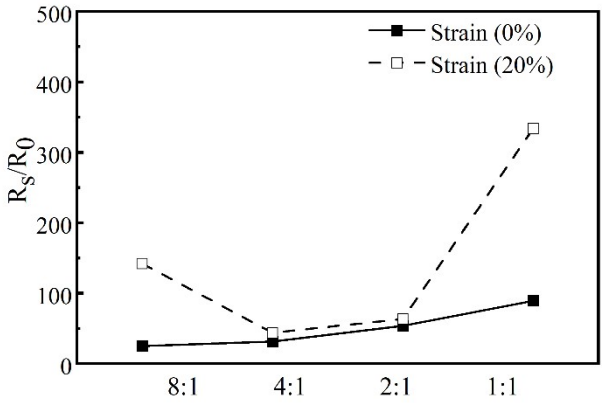

Fig. S3 Normalized sheet resistances of the $Ti_3C_2T_x$-MWCNTs layers with different volume ratios of $Ti_3C_2T_x$ and MWCNTs ink.

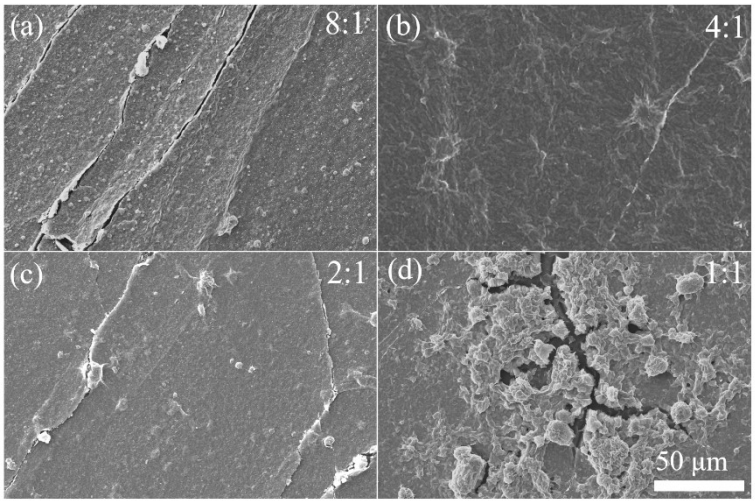

Fig. S4 $Ti_3C_2T_x$-MWCNTs layers with different volume ratios of $Ti_3C_2T_x$ and MWCNTs ink.

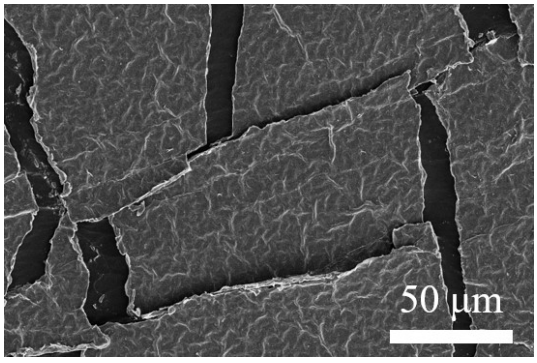

Fig. S5 SEM image of TMS surface without the addition of NMP in $Ti_3C_2T_x$-MWCNTs inks (under 20% strain).

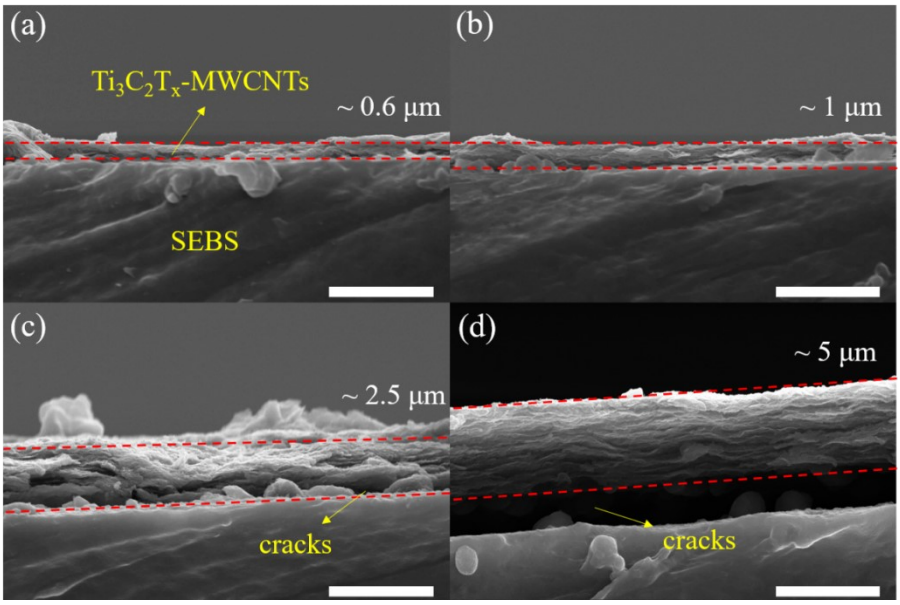

Fig. S6 SEM images of the TMS current collector with different thickness of $Ti_3C_2T_x$-MWCNTs layer. Scale bar: 5 μm.

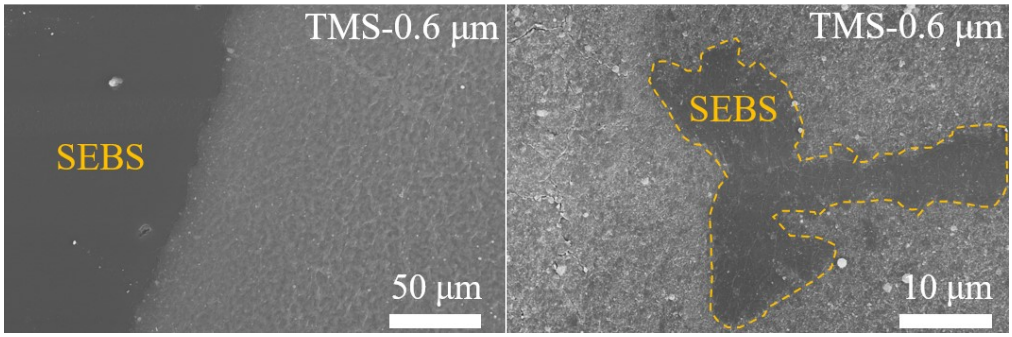

Fig. S7 SEM images of TMS surface with 0.6 μm thickness of $Ti_3C_2T_x$-MWCNTs layer.

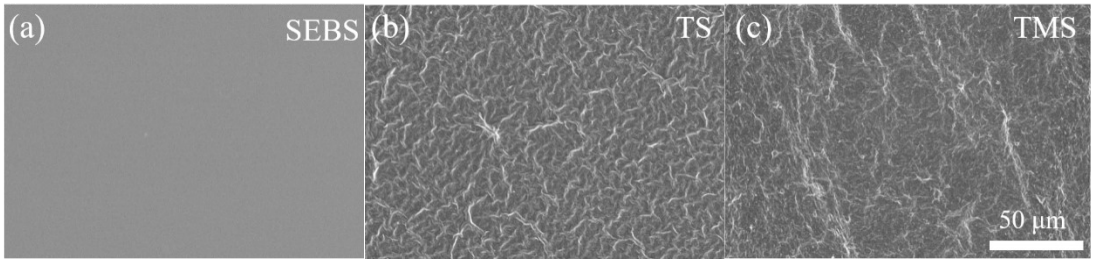

Fig. S8 SEM image of (a) SEBS, (b) TS, and (c) TMS surface.

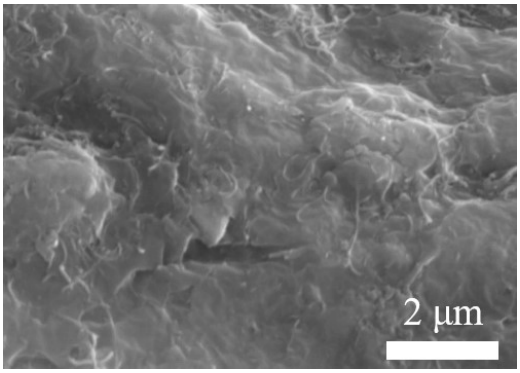

Fig. S9 SEM image of TMS surface.

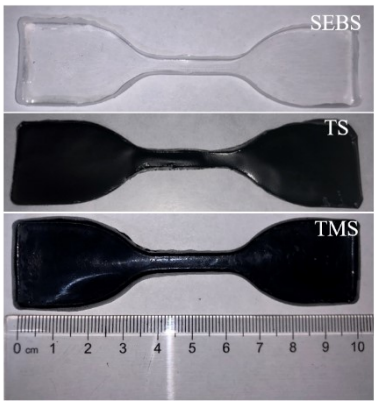

Fig. S10 Images of SEBS, TS, and TMS films.

Table S2. Mechanical properties of SEBS, TS, and TMS films

Sample	Young's Modulus (MPa)	Tensile Strength (MPa)	Strain at break (%)
SEBS	19.19	11.68	742.28
TS	33.42	15.61	781.82
TMS	37.77	15.80	761.45

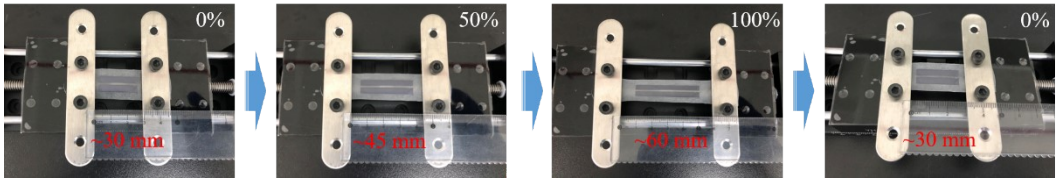

Fig. S11 The optical pictures of the TMS current collector under various strains.

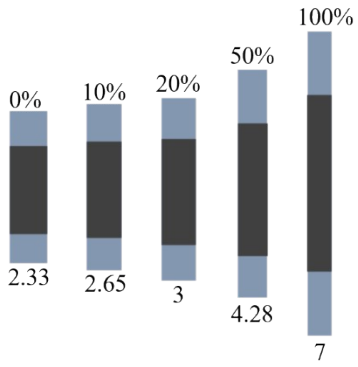

Fig. S12 Schematics of sample strips for the AR measurement. The length and width are measured when the samples are stretched to 0%, 10%, 50%, and 100% strains.

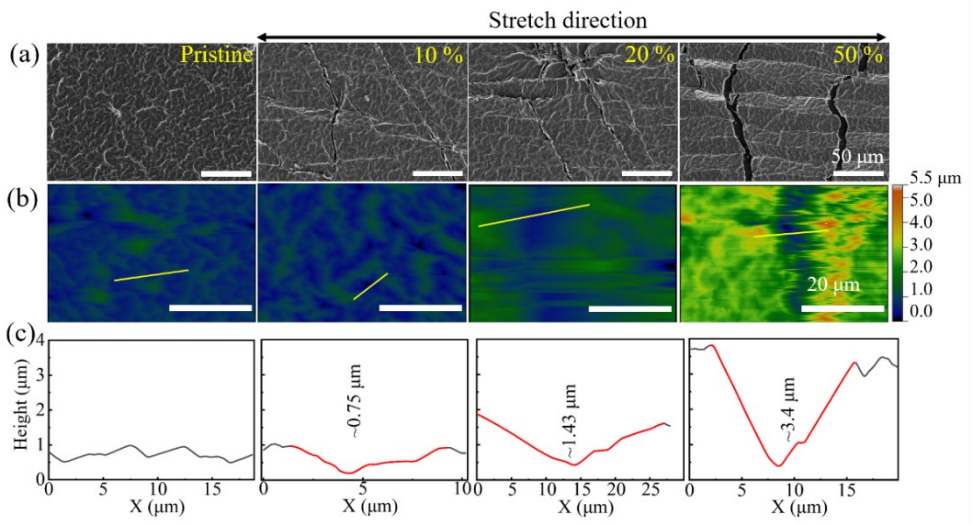

Fig. S13 (a) The SEM images, (b) optical topographic images, and (c) step height measurement of TS surface at different tensile states.

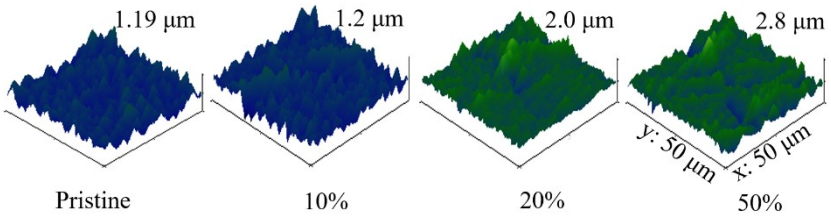

Fig. S14 The 3D optical topographic images of TMS surface at different tensile states.

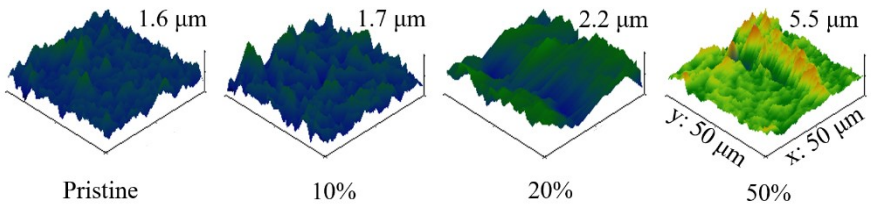

Fig. S15 The 3D optical topographic images of TS surface at different tensile states.

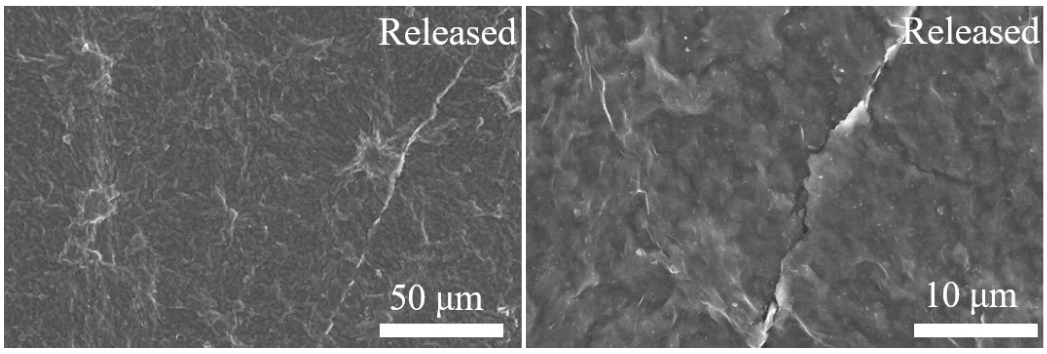

Fig. S16 Superficial SEM image of TMS after removing the stress.

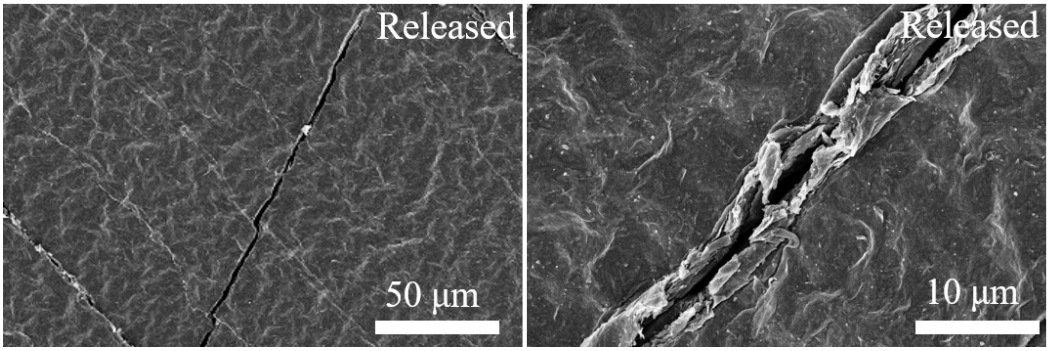

Fig. S17 Superficial SEM image of TS after removing the stress.

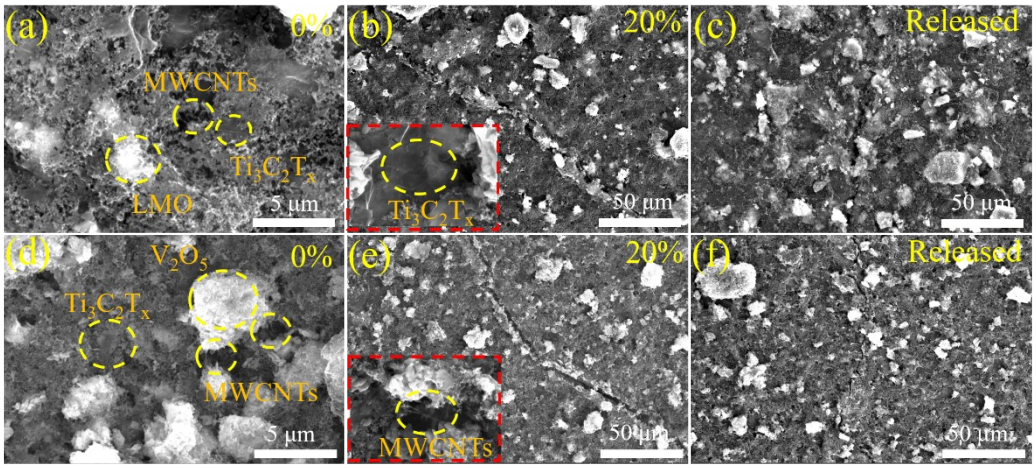

Fig. S18 Superficial SEM images of (a-c) LMO/TMS and (d-f) V_2O_5/TMS electrodes under different strains.

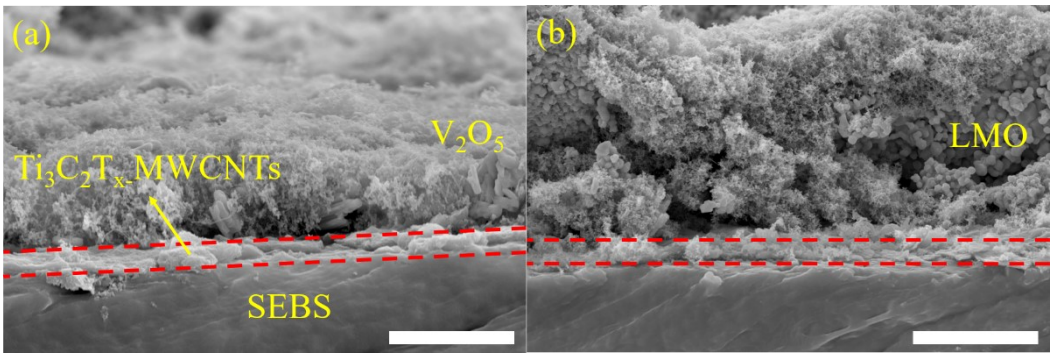

Fig. S19 Cross-sectional SEM images of (a) V_2O_5/TMS and (b) LMO/TMS electrodes. Scale bar: 5 μm.

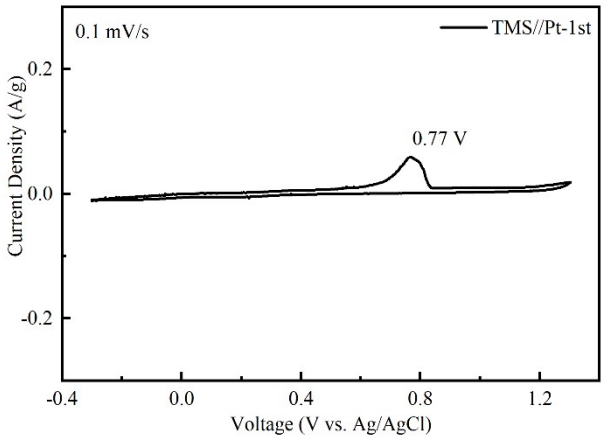

Fig. S20 CV curve of TMS current collector in a three-electrode system in the first cycle.

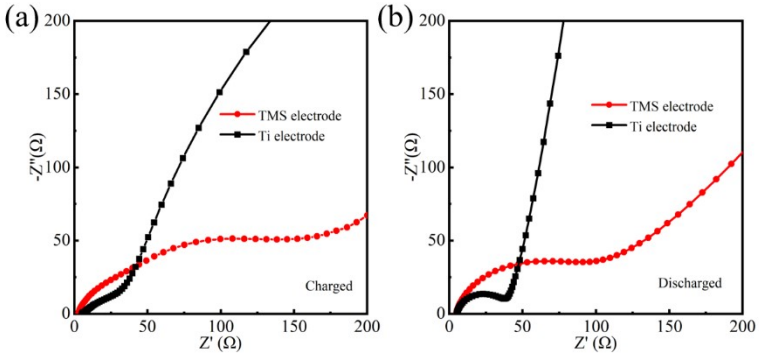

Fig. S21 The EIS curves of TMS-based and Ti foil-based coin cells after charge and discharge, respectively.

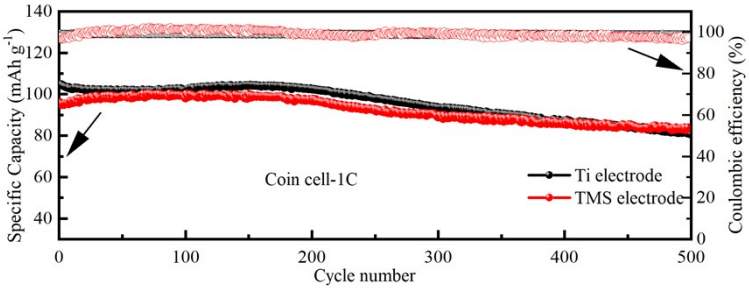

Fig. S22 Capacity retention tests of the TMS and Ti foil-based coin cells at 1C rate

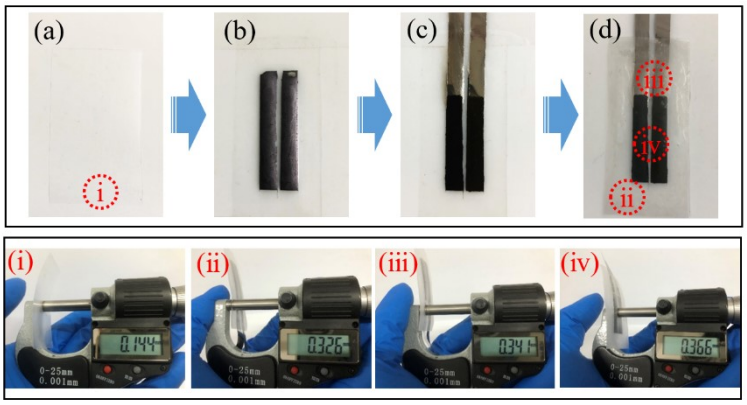

Fig. S23 Thickness measurement of stretchable LIB.

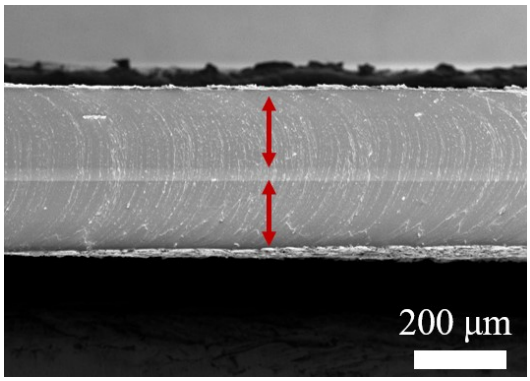

Fig. S24 Cross-sectional SEM image of two combinative SEBS films.

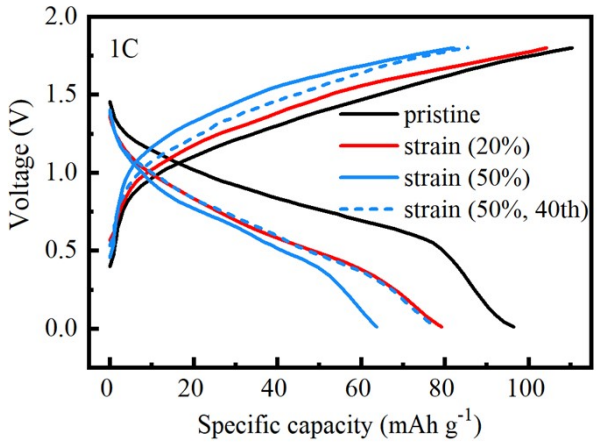

Fig. S25 Charge/discharge curves of the stretchable LIBs at a 1C rate under various strains.

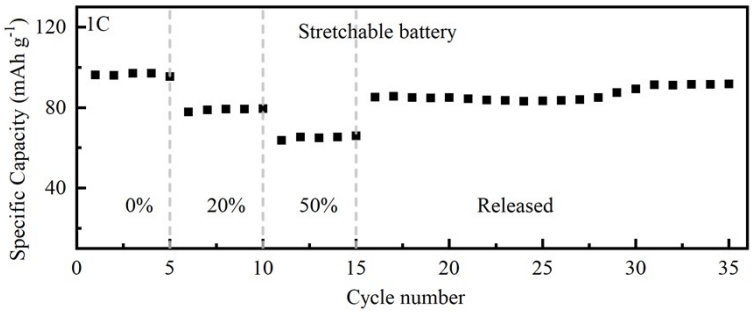

Fig. S26 The cycle stability tests of the stretchable batteries at a current density of 1C under various strains

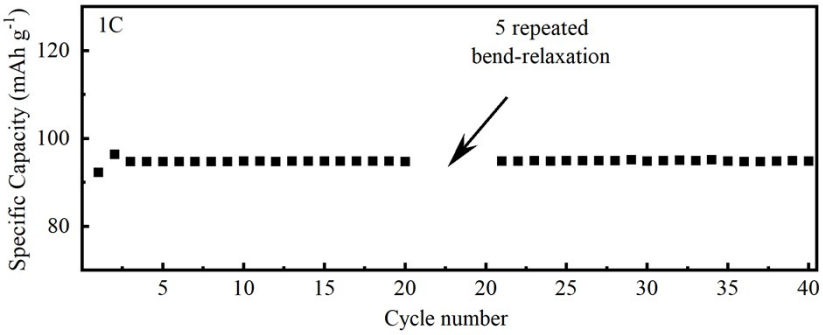

Fig. S27 The cycle stability in response to 5 repeated bend-relaxation cycles at a current density of 1C.

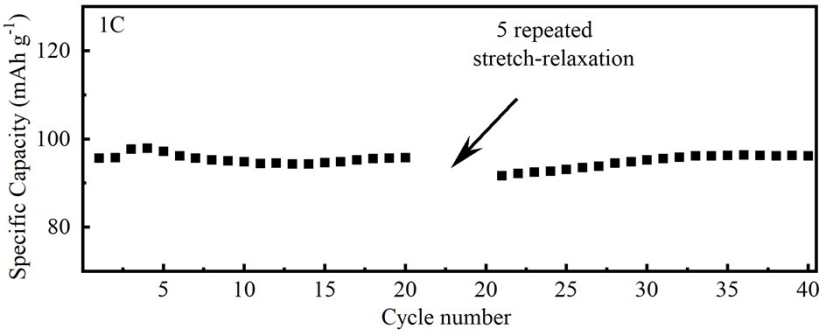

Fig. S28 The cycle stability in response to 5 repeated stretch-relaxation cycles (20% strain) at a current density of 1C.

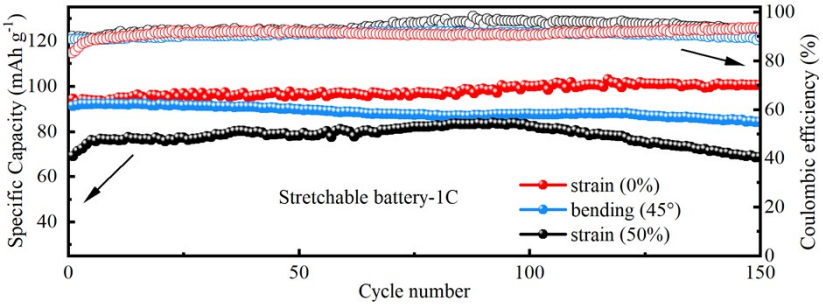

Fig. S29 Capacity retention tests of the stretchable LIBs at a current density of 1C under different tensile states.

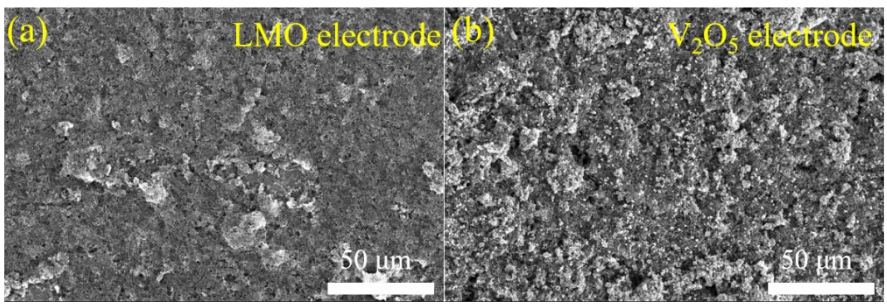

Fig. S30 SEM images of (a) LMO/TMS and (b) V_2O_5/TMS electrodes after cycles.

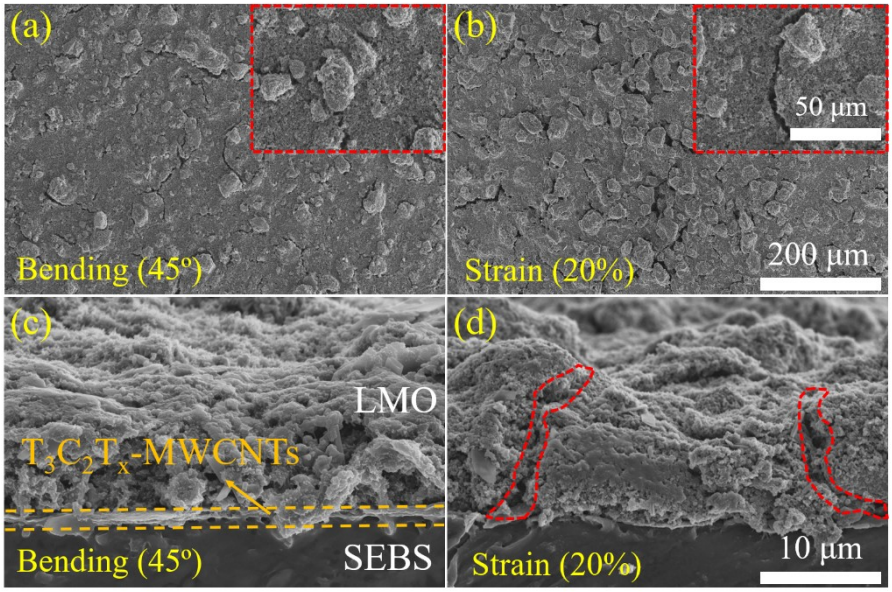

Fig. S31 (a, b) Superficial and (c, d) cross-sectional SEM images of LMO/TMS electrodes after cycles.

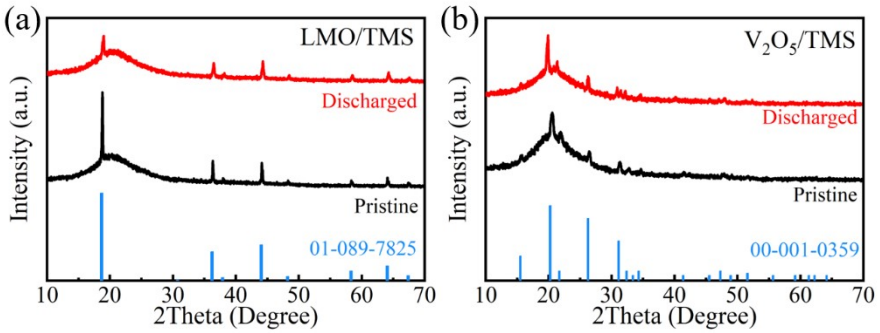

Fig. S32 The XRD patterns of LMO/TMS and V_2O_5/TMS electrodes after discharge.

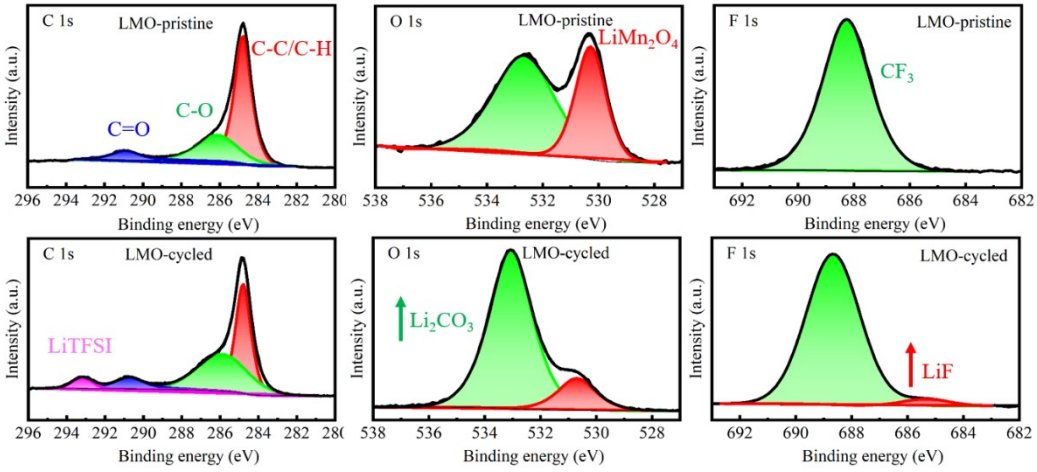

Fig. S33 The XPS spectra (C 1s, O 1s, and F 1s) of LMO/TMS electrodes before and after cycles.

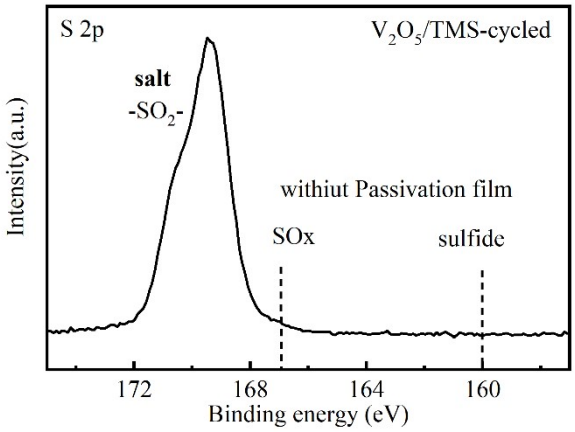

Fig. S34 The XPS spectra (S 2p) of V_2O_5/TMS electrode after cycles.

Table S3. Comparison of the thickness and electrochemical performances of TMS-based full battery with other stretchable batteries

Device type	Materials of current collector	Thickness of current collector	Thickness of whole battery	Capacity/ mAh g^{-1}	Cycles	Large strains
Aqueous LIB (this work)	**$Ti_3C_2T_x$-MWCNTs/SEBS**	**~144 μm**	**~366 μm**	**96.5 (0.1 A g^{-1})**	**300 (0.75 A g^{-1})**	**50%**
Zn-MnO_2[1]	AgNW/MWCNTs -SIS	~80 μm	~425μm	150 (0.5 A g^{-1})	100 cycles (0.1 A g^{-1})	100%
Aqueous LIB[2]	Au NPs-PU	~27 μm	~1 mm	100 (0.5 A g^{-1})	1000 cycles (0.5 A g^{-1})	30%
Aqueous LIB[3]	SEBS-CNT-CB-Ag	~100 μm	>600 μm	53 (0.12 A g^{-1})	50 cycles (0.12 A g^{-1})	50%
Aqueous LIB[4]	Hybrid carbon/polymer	~200 μm	~10 mm	90 (20 C)	500 (20 C)	200%
SIB[5]	PDMS-RGO	~800 μm	>1.6 mm	103 (10 mA g^{-1})	100 (1 C)	50%
Zn-MnO_2 battery[6]	PUS@AgNW	~2 mm	>4 mm	3.6 mAh cm^{-2} (12 mg cm^{-2})	/	100%
LIB[7]	PDMS-SWCNTs	~800 μm	>2 mm	0.81 mAh cm^{-2} (0.069 C)	/	50%
LIB[8]	PMDS sponge	~500 μm	/	120 (34 mA g^{-1})	/	/
Supercapacitor[9]	PEDOT NFs@FKM	~250 μm	>850 μm	/	/	/

	PDAA@Ag NWs/FKM					
LIB[10]	rGO-CNT/active materials	~1.5 cm	~6.5 cm	140 (0.5 C)	100 (0.5 C)	50%
Supercapacitor[11]	$Ti_3C_2T_x$ /RGO-acrylic elastomer substrate	>1 mm	>2 mm	/	/	/
Supercapacitor[12]	Crumpled-CNT-forest-acrylic elastomer substrate	>1 mm	>2 mm	/	/	/
Aqueous LIB[13]	crumpled Ag-NW network	~300 μm	>900 μm	119 (0.2 A g^{-1})	250 (0.2 A g^{-1})	100%
LIB[14]	microscale square array/PDMS	~600 μm	~1.7 mm	121 mAh g^{-2} (1 C)	200 (1 C)	100%
LIB[15]	3D printed porous substrates	>200 μm	/	/	/	/

1. C. Bai, K. Ji, S. Feng, J. Zhang and D. Kong, *Energy Storage Mater.*, 2022, **47**, 386-393.
2. M. Gu, W.-J. Song, J. Hong, S. Y. Kim, T. J. Shin, N. A. Kotov, S. Park and B.-S. J. S. a. Kim, *Sci. Adv.* 2019, **5**, eaaw1879.
3. X. Chen, H. Huang, L. Pan, T. Liu and M. Niederberger, *Adv Mater.*, 2019, **31**, e1904648.
4. W.-J. Song, J. Park, D. H. Kim, S. Bae, M.-J. Kwak, M. Shin, S. Kim, S. Choi, J.-H. Jang, T. J. Shin, S. Y. Kim, K. Seo and S. Park, *Adv.Energy Mater.*, 2018, **8**, 1702478.
5. H. Li, Y. Ding, H. Ha, Y. Shi, L. Peng, X. Zhang, C. J. Ellison and G. Yu, *Adv. Mater.*, 2017, **29**, 1700898.
6. H.-W. Zhu, J. Ge, Y.-C. Peng, H.-Y. Zhao, L.-A. Shi and S.-H. Yu, *Nano Research*, 2018, **11**, 1554-1562.
7. J. Liang, S. Wang, H. Yu, X. Zhao, H. Wang, Y. Tong, Q. Tang and Y. Liu, *Sustainable Energy & Fuels*, 2020, **4**, 2718-2726.
8. W. Liu, Z. Chen, G. Zhou, Y. Sun, H. R. Lee, C. Liu, H. Yao, Z. Bao and Y. Cui, *Adv. Mater.*, 2016, **28**, 3578-3583.
9. H. Mu, W. Wang, L. Yang, J. Chen, X. Li, Y. Yuan, X. Tian and G. Wang, *Energy Storage Mater.*, 2021, **39**, 130-138.
10. S. Kang, S. Y. Hong, N. Kim, J. Oh, M. Park, K. Y. Chung, S. S. Lee, J. Lee and J. G. Son, *ACS Nano*, 2020, **14**, 3660-3668.
11. Y. Zhou, K. Maleski, B. Anasori, J. O. Thostenson, Y. Pang, Y. Feng, K. Zeng, C. B. Parker, S. Zauscher, Y. Gogotsi, J. T. Glass and C. Cao, *ACS Nano*, 2020, **14**, 3576-3586.
12. C. Cao, Y. Zhou, S. Ubnoske, J. Zang, Y. Cao, P. Henry, C. B. Parker and J. T. Glass, *Adv Energy Mater.*, 2019, **9**, 1900618.
13. X. Cao, D. Tan, Q. Guo, T. Zhang, F. Hu, N. Sun, J. Huang, C. Fang, R. Ji, S. Bi and C. Jiang, *J. Mater. Chem. A*, 2022, **10**, 11562-11573.
14. Y. Lu, S. Ru, H. Li, G. Wang and S. Xu, *J Colloid Interface Sci.*, 2023, **631**, 1-7.
15. S. Praveen, T. Kim, S. P. Jung and C. W. Lee, *Small*, 2023, **19**, e2205817.